JACS
JOURNAL OF THE AMERICAN CHEMICAL SOCIETY
Article
pubs.acs.org/JACS

Extreme Synergistic Mutational Effects in the Directed Evolution of a Baeyer–Villiger Monooxygenase as Catalyst for Asymmetric Sulfoxidation

Zhi-Gang Zhang,[†,‡] Richard Lonsdale,[†,‡] Joaquin Sanchis,[§] and Manfred T. Reetz*[,†,‡]

[†]Department of Chemistry, Philipps-Universität Marburg, Hans-Meerwein Str., 35032 Marburg, Germany
[‡]Max-Planck-Institut für Kohlenforschung, Kaiser-Wilhelm-Platz 1, 45470 Mülheim an der Ruhr, Germany
[§]Monash Institute of Pharmaceutical Sciences, Monash University, 381 Royal Parade, Parkville, 3052 VIC, Australia

Supporting Information

ABSTRACT: Structure-based directed evolution utilizing iterative saturation mutagenesis (ISM) has been applied to phenyl acetone monooxygenase (PAMO), a thermally robust Baeyer–Villiger monooxygenase, in the quest to access a mutant which displays reversed enantioselectivity in the asymmetric sulfoxidation of prochiral thioethers. Whereas WT PAMO leads to 90% ee in the sulfoxidation of *p*-methylbenzyl methyl thioether with preference for the (*S*)-sulfoxide, the evolved mutant I67Q/P440F/A442N/L443I is 95% (*R*)-selective in the reaction of this and other thioethers. Partial deconvolution of the (*R*)-selective mutant with generation of the respective four single mutants shows that all of them are (*S*)-selective, which points to pronounced synergism (cooperative nonadditivity) when they interact in concert. Complete deconvolution with formation of all combinatorial forms of the respective double and triple mutants allows the designed construction of a fitness landscape featuring all 24 upward pathways leading from WT to the (*R*)-selective quadruple mutant. In all 24 trajectories strong cooperative mutational effects were found as well, which indicates that such mutational changes in enzymes constitute nonlinear systems. A theoretical analysis based on induced fit docking explains many of the observed effects on a molecular level.

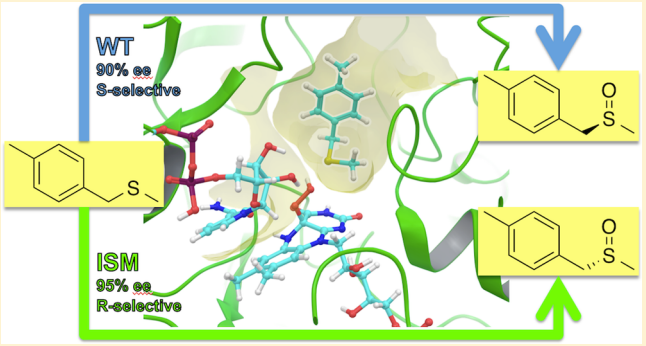

INTRODUCTION

The catalytic asymmetric sulfoxidation of prochiral thioethers constitutes an important transformation in organic chemistry, mediated by chiral synthetic transition metal complexes,[1] organocatalysts,[2] or enzymes of the type Baeyer–Villiger monooxygenases (BVMOs).[3,4] These flavin-dependent enzymes react with molecular oxygen to form an intermediate flavin-hydroperoxide (Fl-OOH) which reacts electrophilically with either one of the two enantiotopic lone electron pairs (or both) of the sulfur functionality.[4] In contrast, the Baeyer–Villiger reaction is initiated by nucleophilic addition of deprotonated flavin-hydroperoxide ($Fl\text{-}OO^-$) to the carbonyl function of ketones with formation of a short-lived Criegee intermediate.[3,5] Stereodifferentiation between the two lone electron pairs of prochiral thioethers can be achieved by using wildtype (WT) cyclohexanone monooxygenase (CHMO)[3,4] or mutants for "difficult" substrates,[6] but this BVMO is only moderately thermostable, requiring immobilization and other biotechnological techniques for practical applications.[3j] In contrast, phenyl acetone monooxygenase (PAMO) is an exceptionally robust BVMO.[7] Unfortunately, wildtype (WT) PAMO generally shows low degrees of enantioselectivity in the oxidation of most thioethers.[8] Utilizing the crystal structure of PAMO,[9] Mihovilovic, Fraaije and co-workers applied rational design in the successful attempt to enhance (*R*)-selectivity significantly in these cases, variant M446G leading to 92–95% *ee* for several thioethers.[10] However, reversal of stereoselectivity has not been achieved to date.

Here we report a directed evolution[11] study, which provides both (*R*)- and (*S*)-selective PAMO variants for several structurally different thioethers. We also made the surprising discovery that upon deconvoluting the best (*R*)-selective mutant characterized by four point mutations, all of the respective single mutants are (*S*)-selective. This is the most extreme case of cooperative nonadditivity recorded thus far in protein engineering,[12] an unusual phenomenon that inspired us to construct a complete fitness landscape featuring all 4! = 24 pathways leading from WT PAMO to the best (*R*)-selective mutant, which likewise revealed drastic nonadditivity in all of the upward evolutionary trajectories. In an attempt to unveil the source of enantioselectivity, induced fit docking calculations were applied.

Received: September 23, 2014
Published: November 14, 2014

   dx.doi.org/10.1021/ja5098034 | J. Am. Chem. Soc. 2014, 136, 17262–17272

RESULTS AND DISCUSSION

Experimental Platform and Initial Results Using a Model Substrate. The asymmetric sulfoxidation of thio-ether **1b** was chosen as the model reaction (Scheme 1), with WT

Scheme 1. Model Reaction Used in all Protein Engineering Experiments

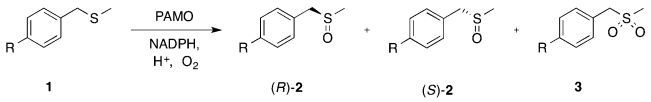

PAMO leading to (*S*)-**2b** with high enantioselectivity (90% *ee*), similar to the sulfoxidation of substrate **1a** (99% *ee* in favor of (*S*)-**2a**).[8] Prior to applying directed evolution for improving (*S*)-selectivity and reversing enantioselectivity in favor of (*R*)-**2b**, we first tested 40 different PAMO mutants that have been previously evolved for stereoselective BV reactions[13] (Supporting Information). Most of these variants proved to be (*S*)-selective. Some of the most (*S*)-selective variants, together with the two slightly (*R*)-selective variants, are shown in Table 1,

Table 1. Best (*S*)- and (*R*)-Selective PAMO Mutants (Lysates) as Catalysts in the Asymmetric Sulfoxidation of Thioether 1b, All Originating from Previous PAMO Studies Regarding Stereoselective BV Reactions[13] (Experimental Uncertainty in the %*ee*-Values Here and in All Other Stereoselectivity Data Is Better than ±2%)

entry	variant	% conversion	% *ee*	config.	% sulfone
1	Q93N	99	96	*S*	6
2	Q93N/P94D	89	92	*S*	6
3	L443F	99	95	*S*	12
4	P440A	99	99	*S*	16
5	P440V	99	95	*S*	11
6	P440D	99	98	*S*	3
7	P440E	99	94	*S*	5
8	P440W	86	97	*S*	6
9	P440T	99	93	*S*	13
10	P440Y	85	10	*R*	11
11	P440L	75	5	*R*	22
12	P440F	82	56	*S*	23

where lysates were used in all cases. Depending upon the nature of the variant, and the conditions used, some degree of overoxidation with formation of the respective sulfone **3** was observed in most cases. This means that kinetic resolution of the sulfoxides may be operating, which could influence the apparent ee-value, a commonly observed feature in BVMO-catalyzed sulfoxidation reactions.[6]

In order to achieve high levels of reversed enantioselectivity, we turned to directed evolution[11] using iterative saturation mutagenesis (ISM).[11f,14] Guided by the crystal structure of PAMO,[9] and by previously identified "hot spots" (CAST sites),[13] we considered the loop residues P440, A442, and L443 as potential randomization sites for saturation mutagenesis, in addition to V54, I67, Q152 identified earlier as "hot spots" by Mihovilovic, Fraaije and co-workers[10] (Figure 1).

One of several strategies would be to group these single amino acid positions into multiresidue saturation sites,[14] e.g., three 2-residue sites with application of ISM, six upward

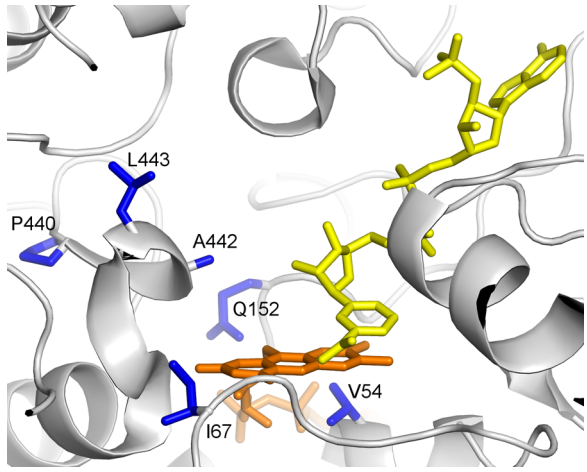

Figure 1. Potential randomization sites (blue) in PAMO. The flavin and NADP cofactors are displayed in orange and yellow, respectively. Based on the 2YLX crystal structure of PAMO.[15]

pathways being possible. In order to keep the screening effort as low as possible, we first performed exploratory experiments by focusing saturation mutagenesis separately at the following residues: V54, I67, Q152, and A442. WT PAMO and the P440Y mutant (showing 10% (*R*)-selectivity) were used as templates in two separate series of experiments. Instead of applying conventional NNK codon degeneracy encoding for all 20 canonical amino acids, the "smart-intelligent" library construction strategy for avoiding amino acid bias reported by Tang[16a] was used as an alternative to the 22c trick applied previously to P450 monooxygenses.[16b] This technique involves four pairs of primers with degenerate codons of NDT (encoding 12 amino acids N, S, I, H, R, L, Y, C, F, D, G, and V), VMA (encoding 6 amino acids E, A, Q, P, K, T), and ATG (encoding M) as well as TGG (encoding W) at the target sites, which were mixed in a ratio of 12:6:1:1. Saturation mutagenesis at residue V54 failed to yield improved variants, in contrast to randomization at positions 67, 152, and 442 (Table 2). In each case, only 60 variants had to be screened for complete library coverage.

In addition to improved (*S*)-selectivity (Table 2, entries 22–26), several variants with increased (*R*)-selectivity were identified (Table 2, entries 5–8, 14–21), which indicates that positions 67, 152, and 442 appear to be "hot spots". The best (*R*)-selective variant proved to be I67T/P440Y (82% *ee*), originating from randomization at position 67 using mutant P440Y as a template. It was then used as a template for saturation mutagenesis at site A442/L443, but this failed to deliver a notably improved (*R*)-selective variant. Rather than applying the previously developed strategy for escaping from local minima by utilizing an inferior mutant for further ISM experiments,[14c] we chose a different strategy.

The plan was to apply ISM, with WT PAMO serving as the template and P440/A442/L443 as the initial 3-residue randomization site (site A). These residues belong to part of a loop that was known to be sensitive to mutational changes in stereoselective BV reactions.[7,10,13] NNK codon degeneracy encoding of all 20 canonical amino acids would require considerable oversampling in the screening step, in order to achieve 95% coverage (~98 000 transformants) according to traditional statistics.[14,17] In order to minimize such efforts, reduced amino acid alphabets were chosen.[14] Table 1 reveals

dx.doi.org/10.1021/ja5098034 | J. Am. Chem. Soc. 2014, 136, 17262–17272

Table 2. Best Variants for Substrate 1b Identified by Saturation Mutagenesis (Using Lysates) at Amino Acid Positions 67, 152, and 442[a]

entry	mutant	% conversion[b]	% *ee*	config.	% sulfone
1	WT	62	91	*S*	7
2	A442S	ND	83	*S*	8
3	A442D	ND	49	*S*	16
4	A442Y	ND	56	*S*	11
5	A442F/P440Y	63	61	*R*	5
6	A442T/P440Y	99	57	*R*	12
7	A442H/P440Y	99	55	*R*	4
8	A442Q/P440Y	99	36	*R*	3
9	I67T	55	44	*S*	3
10	I67G	24	61	*S*	1
11	I67A	18	52	*S*	1
12	I67S	51	70	*S*	2
13	I67L	99	70	*S*	3
14	I67T/P440Y	99	82	*R*	7
15	I67E/P440Y	99	79	*R*	1
16	I67G/P440Y	99	72	*R*	6
17	I67A/P440Y	99	76	*R*	2
18	I67F/P440Y	99	70	*R*	1
19	I67Q/P440Y	99	65	*R*	2
20	I67Y/P440Y	99	69	*R*	1
21	I67C/P440Y	99	60	*R*	6
22	Q152I	62	97	*S*	1
23	Q152V	50	97	*S*	1
24	Q152S	49	97	*S*	1
25	Q152M	57	97	*S*	1
26	Q152A	49	97	*S*	1

[a]Further variants are detailed in the Supporting Information (Table S2). [b]ND = not determined.

that the single mutants P440Y and P440L cause a slight reversal of enantioselectivity in favor of (*R*)-**2**, and P440F reduces (*S*)-selectivity considerably. Thus, for position 440 only these three amino acids were chosen as building blocks (Y, L, and F). At positions 442 and 443, NDT codon degeneracy was used. Taking all three positions together, the choice of the designed reduced amino acid alphabets requires the screening of about 1700 transformants for 95% library coverage. We screened 900 transformants, corresponding to ~80% library coverage, which provided six variants showing (*R*)-selectivity in the range 70–75% *ee* (Supporting Information, Table S3). The subsequent site to be targeted was residue I67, this position also being a "hot spot" (site B). In principle, any individual one of the six best mutants originating from library A could be employed as a template for saturation mutagenesis. Instead, we employed all six of them simultaneously, because this increases structural diversity, while keeping screening at a minimum (20 × 3 × 6 = 360 transformants for 95% library coverage). In order to eliminate amino acid bias, the method of Tang was used once more. Upon screening only 90 transformants, several improved variants were identified, the two best ones being I67C/P440F/A442F/L443D (Variant ZGZ-1) and I67Q/P440F/A442N/L443I (Variant ZGZ-2), showing enantioselectivities of 92% *ee* and 95% *ee*, respectively, in favor of (*R*)-**2**. The resulting experimental ISM scheme featuring pathway A → B which provides two excellent variants is shown in Figure 2. The change in free energy $\Delta\Delta G^{\ddagger}$ associated with reversing enantioselectivity upon going from WT PAMO (90% *ee S*) to variant ZGZ-2 (95% *ee R*) is considerable,

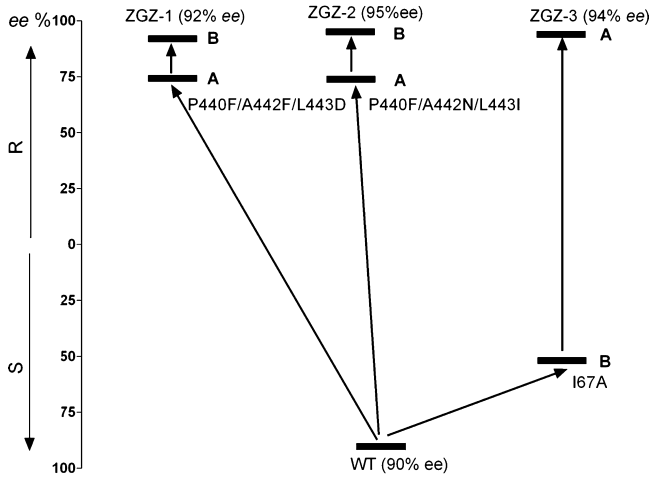

Figure 2. ISM scheme in the directed evolution of PAMO as a catalyst in the asymmetric sulfoxidation of substrate **1b** with preferential formation of (*R*)-**2b**.

amounting to 16.4 kJ/mol (7.3 kJ/mol + 9.1 kJ/mol; see Table 6).

In view of the high degree of stereoselectivity, visiting further randomization sites (Figure 1) was not necessary. However, it was of methodological interest to test the alternative pathway B → A. The initial saturation mutagenesis library was created at site B with WT plasmid serving as the template. Three mutants I67C, I67A, and I67T with reduced *S*-selectivity (and therefore going in the right direction) were found after screening only 90 colonies for 95% library coverage. To explore the reverse pathway B → A, site A was revisited with the same codon degeneracy as before, with mutants I67C, I67A, and I67T serving as templates. A screening of 900 transformants revealed one quadruple mutant I67A/P440Y/A442V/L443I (ZGZ-3) with 94% *ee* (Figure 2). In theory, mutant ZGZ-1 should be found in this library. Since only 900 transformants were screened corresponding to low library coverage (3 × 1700 = 5100 transformants for 95% coverage), this result need not come as a surprise. Table 3 summarizes the final results of exploring the two ISM pathways (data from reaction by purified enzymes).

Table 3. Best (*R*)-Selective PAMO Mutants as Catalysts in the Asymmetric Sulfoxidation of the Model Compound 1b[a]

variant	% conversion	% *ee*	config.	% sulfone
ZGZ-1	96	92	*R*	14
ZGZ-2	97	95	*R*	6
ZGZ-3	99	94	*R*	12

[a]Data using purified enzymes.

Thermostability Tests. In order to check whether the mutational changes influence thermal stability adversely, the T_{50}^{60} values were measured, the temperature at which 50% of the residual activity in the reaction of substrate **1b** remains after a heat treatment for 1 h.[17] Thermally robust WT PAMO has a T_{50}^{60} value of 57.6. Table 4 shows that, with the exception of variant ZGZ-1, no significant reduction in thermostability occurs due to the respective mutational changes.

Determination of Kinetic Parameters. Kinetic parameters were measured for selected PAMO mutants as catalysts in the sulfoxidation of substrate **1b**. The usual UV/vis

dx.doi.org/10.1021/ja5098034 | J. Am. Chem. Soc. 2014, 136, 17262–17272

Table 4. T^{60}_{50} Values (°C) of Selected Purified PAMO Variants

entry	variant	T^{60}_{50}
1	WT	57.6
2	Q152I	56.2
3	Q152V	57.4
4	Q152S	56.6
5	Q152M	56.4
6	Q152A	57.8
7	ZGZ-1	53.2
8	ZGZ-2	56.4

experimental setup measuring the consumption of NADPH as a function of time was used throughout. The results reveal that the k_{cat}/K_m values vary considerably, with in almost all cases catalytic efficiency being greater than that of WT PAMO (Table 5). The lower K_m value of variant ZGZ-1 plays an important role, but thus far we are not able to identify the effect at the molecular level. Whereas induced fit docking computations proved to be useful in understanding nonadditive mutational effects (see below), we decided not to perform such studies for ZGZ-1 because, to the best of our knowledge, it is currently not possible to calculate K_m values to a sufficient level of accuracy that would explain experimental differences of a single order of magnitude.

Table 5. Kinetic Parameters of Selected PAMO Mutants as Catalysts in the Sulfoxidation of Thioether 1b

entry	mutant	selectivity	K_m (mM)	k_{cat}. (s^{-1})	k_{cat}/K_m (M^{-1} s^{-1})
1	WT	*S*	0.58	0.22	371
2	Q152I	*S*	0.43	0.61	1413
3	Q152V	*S*	1.26	0.97	768
4	Q152S	*S*	0.29	0.39	1351
5	Q152M	*S*	0.78	0.92	1175
6	Q152A	*S*	0.29	0.30	1038
7	ZGZ-1	*R*	0.04	0.14	3649
8	ZGZ-2	*R*	0.37	0.69	1879

Deconvolution Experiments of Best Quadruple Mutant ZGZ-2. Studies that focus on uncovering (or predicting) the effect of a single point mutation on the catalytic profile of an enzyme enrich our understanding of biocatalytic mechanisms. The situation becomes more complex when introducing two point mutations, because the question of so-called additivity versus nonadditivity arises.[12] When additivity pertains, for example when considering enzyme activity, the influence of the two respective separate point mutations add up mathematically when they are combined in a double mutant. This means that they do not interact with one another on a molecular level. Fersht[18a] and later Wells[18b] were the first to study such thermodynamic cycles in order to address mechanistic questions, the two initial single mutants being combined with formation of the respective double mutant. Initially, the majority of cases studied using various enzymes led to the conclusion that additivity holds,[18b] but as time went on, a few exceptions were noted.[19] Accordingly, the enzyme activity of the double mutant may prove to be either higher or lower than expected on the basis of a mathematically additive influence of the two single mutations.

In directed evolution, a double mutant constitutes the simplest case in which additivity or nonadditivity can be studied. Deconvolution provides a means to assess the individual catalytic contributions of both point mutations. When more than two mutations are involved, complete deconvolution requires the study of all individual point mutations and of relevant combinatorial sets of mutations.[12,20] Influenced by new experimental data,[20] we recently postulated that nonadditive effects may be more common than traditionally assumed and that for this reason proteins behave as nonlinear systems when multiple mutations are introduced.[12] In such cases a sound theoretical analysis of the effects provides valuable mechanistic and structural information.[20]

We performed deconvolution of the best quadruple mutant ZGZ-2 (I67Q/P440F/A442N/L443I), which shows high (*R*)-selectivity in the sulfoxidation of substrate **1b** (Table 3). Conventional site directed mutagenesis using the QuikChange protocol of Stratagene was applied,[21] and the results are summarized in Table 6. It should be noted that purified variant P440F leads to high (*S*)-selectivity (97% ee), whereas the ee-value resulting from the use of the lysate is only 56% (Table S1). This can be explained by the difference in reaction

Table 6. Results of Deconvoluting PAMO Quadruple Mutant ZGZ-2 as Catalysts (as Purified Enzymes) in the Asymmetric Sulfoxidation of Thioether 1b*

code	mutant	% conversion	% *ee*	config.	% sulfone	$-\Delta\Delta G^{\ddagger}$ (kJ/mol)
	WT-PAMO	69	90	*S*	0	7.3
abcd	I67Q/P440F/A442N/L443I (ZGZ-2)	97	95	*R*	6	9.1
a	I67Q	70	69	*S*	10	4.2
b	P440F	96	97	*S*	59	10.4
c	A442N	54	69	*S*	4	4.2
d	L443I	96	98	*S*	23	11.4
ab	I67Q/P440F	90	73	*R*	5	4.6
ac	I67Q/A442N	26	24	*S*	19	1.2
ad	I67Q/L443I	41	81	*S*	12	5.6
bc	P440F/A442N	95	75	*R*	14	4.8
bd	P440F/L443I	94	73	*S*	32	4.6
cd	A442N/L443I	80	54	*S*	6	3.0
abc	I67Q/P440F/A442N	98	90	*R*	3	7.3
abd	I67Q/P440F/L443I	88	70	*R*	15	4.3
acd	I67Q/A442N/L443I	15	38	*S*	27	2.0
bcd	P440F/A442N/L443I	70	71	*R*	4	4.4

dx.doi.org/10.1021/ja5098034 | J. Am. Chem. Soc. 2014, 136, 17262−17272

conditions and the fact that this particular variant leads to significant overoxidation with formation of the sulfone, which involves kinetic resolution of the chiral sulfoxide.

The deconvolution results are remarkable for several reasons. Variant ZGZ-2 is highly (*R*)-selective (95% *ee*), yet the four respective single mutants show opposite enantioselectivity in favor of (*S*)-**2b**, some with very high *ee*-values (P440F and L443I) as summarized in Table 6. All of the possible double and triple mutants which are combinatorially possible using the four point mutations of variant ZGZ-2 were generated and tested in the model reaction. Here again a number of unusual results were observed which do not correspond to traditional additive mutational effects.[12] For example, not only are the four single mutants (*S*)-selective, but also the double mutant A442N/L443I (54% *ee*) and the triple mutant I67Q/A442N/L443I (38% *ee*) as well. Only upon addition of the fourth point mutation P440F to the latter does drastic inversion to (*R*)-selectivity (variant ZGZ-2) occur. In contrast, the double combinations I67Q/P440F and P440F/A442N lead to inverted (*R*)-selectivity, which likewise signals cooperative nonadditive mutational effects.

Had the four single mutants been generated separately and not originated from deconvolution of an evolved quadruple variant, no researcher would have combined them in the hope of reversing the sense of stereoselectivity in favor of (*R*)-**2b**! Combining the mutations of improved variants has been used in directed evolution numerous times in the hope of improving further a given catalytic property (e.g., enantioselectivity),[11,22] but failures have also been noted[22] (which unfortunately in other cases are not always reported). Therefore, combining "positive" mutations may or may not result in the targeted biocatalyst improvement. Moreover, the present data suggests that combining "deleterious" mutations may in fact provide variants displaying highly improved catalytic profiles, but predicting such combinations is currently a difficult task. A step in this direction is to generate an understanding of the effects that cause the observed strong nonadditive synergistic effects.

Constructing a Fitness Pathway Landscape. For a tutorial on the construction and interpretation of fitness pathway landscapes, see ref 23. The data derived from complete deconvolution of the quadruple mutant I67Q/P440F/A442N/-L443I (ZGZ-2) (Table 6) lead to difficulty in representing a conventional fitness landscape, consisting of a five-dimensional surface in which the four point mutations of variant ZGZ-2 are independent vectors and $\Delta\Delta G^{\ddagger}$ constitutes the dependent variable.

Therefore, we have designed the construction of an experimental fitness pathway landscape characterized by all 4! = 24 pathways (trajectories) leading from WT PAMO to ZGZ-2. In a previous study we utilized this type of approach, an evolved enantioselective mutant of an epoxide hydrolase mutant being the focus of interest. In that deconvolution investigation, all 5! = 120 theoretically possible trajectories were mapped by stacking the respective steps from top (WT) to bottom (best mutant).[23] We have since realized that it is graphically more appealing to stack the steps of such trajectories upward starting from WT (bottom) and ending at the evolved highly enantioselective mutant (top), which represents an upward climb. In the present study we have chosen this graphical representation. For simplicity, we denote the four mutations as follows:

I67Q = a; P440F = b; A442N = c; L443I = d

We first generated the mutants that are relevant when considering all combinations of mutations obtained successively in the previous ISM experiments (Figure 3). Following their assessment regarding enantioselectivity, the free energy values were used in the construction of the 24 upward pathways.

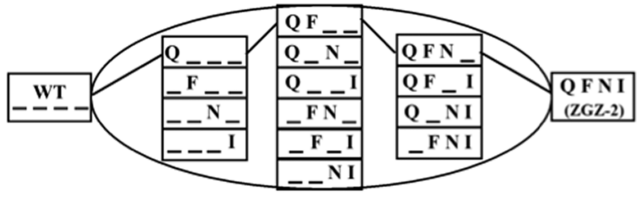

Figure 3. 14 possible mutants in the evolutionary protein space between WT and ZGZ-2. Lines indicate only one trajectory of the 24 combinatorial possibilities to go from WT to ZGZ-2 (Q = a, F = b, N = c, I = d).

The result of this analysis, based on experimental data, is depicted in Figures 4 and 5. It can be seen that six pathways are

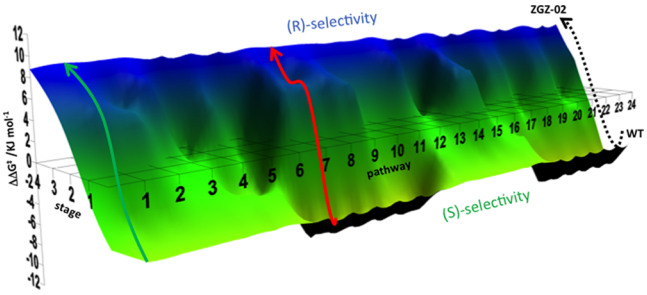

Figure 4. Fitness pathway landscape showing the 24 pathways leading from WT PAMO (bottom) to best (*R*)-selective variant ZGZ-2, a typical trajectory lacking local minima (green pathway) and one having local minima (red) being featured.

energetically "favored" displaying smooth upward climbs, while the majority (18 trajectories) are characterized by local minima. Of course, due to the designed construction of the fitness pathway landscape, all 24 trajectories terminate at variant ZGZ-2.

Figures 4 and 5 illustrate that epistatic interactions occur between individual point mutations and sets of point mutations. Among the features of interest is the influence of mutation d (L443I). Whereas it consistently impedes upward climbs in early phases, it is always required in the final result (ZGZ-2). In order to analyze the cumulative effects quantitatively in any given upward pathway, we applied a previously developed procedure.[23] In the present case, the experimental data in Table 6 were used to calculate the free energy of interaction ($\Delta G^{\ddagger}_{ij}$) between any two mutations or two sets of mutations, designated as *i* and *j* according to eq 1, where $\Delta\Delta G^{\ddagger}_{i}$, $\Delta\Delta G^{\ddagger}_{j}$, and $\Delta\Delta G^{\ddagger}_{exp}$ are the experimentally determined differences in activation energies for the formation of both enantiomers using mutants *i*, *j*, and the binary combination of *i* and *j*, respectively. This thermodynamic cycle is in analogy to the scheme originally suggested by Fersht[17] regarding the interaction of two point mutations.

$$\Delta G^{\ddagger}_{ij} = \Delta\Delta G^{\ddagger}_{exp} - (\Delta\Delta G^{\ddagger}_{i} + \Delta\Delta G^{\ddagger}_{j}) \quad (1)$$

dx.doi.org/10.1021/ja5098034 | J. Am. Chem. Soc. 2014, 136, 17262−17272

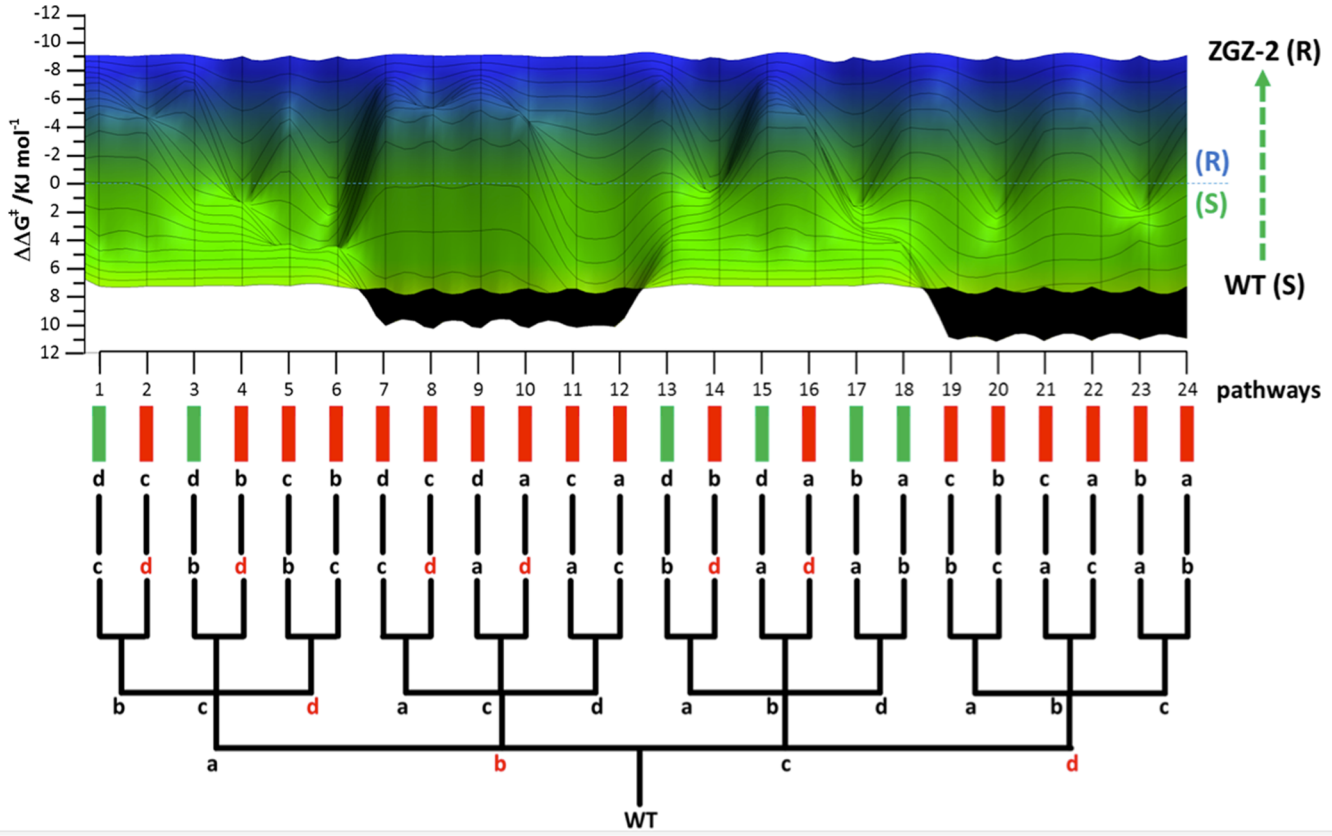

Figure 5. Fitness pathway landscape in the frontal view of Figure 4 of all 24 trajectories leading from WT PAMO to variant ZGZ-2 characterized by four point mutations. Green notations indicate energetically favored pathways, whereas red notations represent disfavored trajectories having local minima. Letters in red in the dendrogram denote a local minimum after the introduction of this mutation.

For illustrative purposes, a green pathway, a → b → c → d (Figure 6), and a red one, d → a → b → c (Figure 7), are

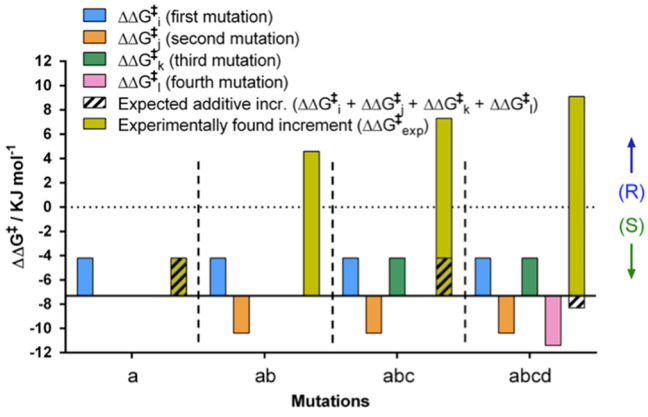

Figure 6. Thermodynamic cycle (eq 1) highlighting the interaction of point mutations and sets of mutations involved at every stage along the energetically favored pathway a → b → c → d toward variant ZGZ-2 as a catalyst in the sulfoxidation of substrate **1b**.

analyzed here (see Supporting Information for other trajectories). Figure 6 shows that in the initial phase of the energetically favored pathway the first mutation causes a slight decrease in (*S*)-selectivity, but the second mutation alone causes a shift in the wrong direction, i.e., (*S*)-selectivity increases relative to WT. Functioning in concert, reversal of enantioselectivity in favor of the (*R*)-manifold is induced. If

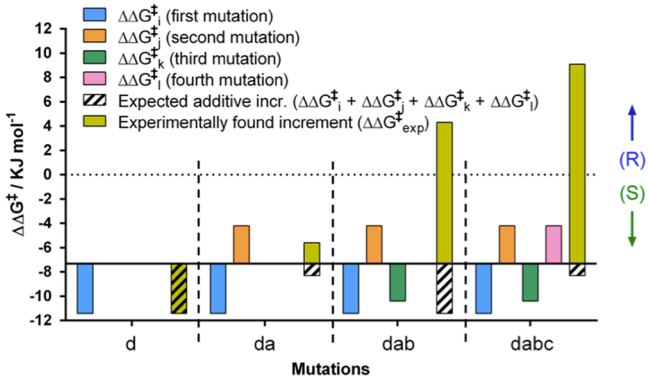

Figure 7. Thermodynamic cycle (eq 1) highlighting the interaction of point mutations and sets of mutations involved at every stage along the energetically disfavored pathway d → a → b → c toward variant ZGZ-2 as a catalyst in the sulfoxidation of substrate **1b**.

mathematical additivity had pertained, then the respective double mutant would show about the same (*S*)-selectivity as WT PAMO. The cooperative interaction between the two point mutations amounts to about 4 kJ/mol. Strong cooperativity also operates at all other points along this pathway; in the final step, $\Delta G_{ij}^{\ddagger}$ amounts to about 10 kJ/mol. In the case of pathway d → a → b → c (Figure 7), pronounced cooperative mutational effects are also visible (as in all of the 24 trajectories).

Uncovering the Reasons for Nonadditive Mutational Effects. In an attempt to rationalize the observed nonadditive

dx.doi.org/10.1021/ja5098034 | J. Am. Chem. Soc. 2014, 136, 17262−17272

effects favoring cooperativity (synergy), induced fit docking calculations[5,24] were performed with the model substrate **1b**, on the WT enzyme, along with the mutant enzymes detailed in Table 7. The FAD-OO^- species has been suggested to be the

Table 7. Mutants of PAMO Studied with Model Substrate 1b by Induced Fit Docking[a]

mutant	predicted selectivity	observed selectivity	r(O–S) [Å]
WT	*S*	*S*	4.16
P440F	*S*	*S*	5.35
L443I	*S*	*S*	5.78
P440F/L443I	*S*	*S*	5.64
I67Q/P440F/L443I	*R*	*R*	5.55
ZGZ-2	*R*	*R*	3.66

[a]Predicted selectivity is based on the orientation of the substrate in the active site. Observed selectivity is based on experimental ee-value (Table 6). Distance between the substrate sulfur and the hydroperoxo oxygen furthest from the FAD cofactor (r).

oxidizing species for the Baeyer–Villiger reaction catalyzed by cyclohexanone-monooxygenase (CHMO). This reaction has been studied previously using QM/MM calculations.[5] As the precise mechanism and oxidizing species responsible for sulfoxidation of thioethers have yet to be elucidated, the FAD cofactor was modeled in the hydroperoxo form (FAD-OOH). The likely oxidizing species for thioethers are the FAD-OOH or FAD-OO^- moieties. A QM/MM mechanistic study may shed light on this issue, but is beyond the scope of the current work. Our primary goal here is to explore the effect of the mutations on the binding orientation of the substrate within the active site, which will in turn aid in predicting the selectivity of sulfoxidation. We assume that the closest of the two sulfur lone pairs to the –OOH moiety will be the one that undergoes oxidation, yielding either (*R*)- or (*S*)-**2b** (Figure 8).

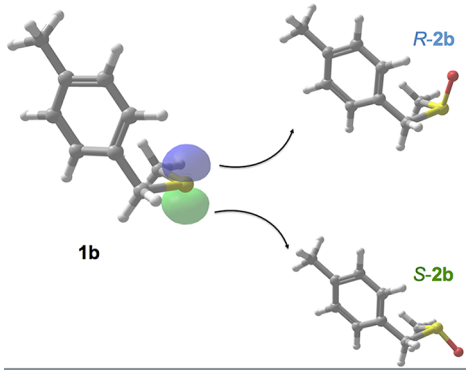

Figure 8. Oxidation of **1b** by PAMO. Oxidation at the blue and green lone pairs will lead to formation of *R*- and *S*-**2b**, respectively.

A range of binding poses were obtained for each mutant. Poses were considered for analysis where a distance of less than 6 Å was observed between the substrate sulfur and the hydroperoxo oxygen furthest from the FAD cofactor. Binding poses of **1b** in the active site of the WT and selected mutants are depicted in Figure 9. These poses are those in which the highest induced fit docking score was obtained. The observed binding poses of substrate **1b** in the active site for all of the simulated mutants are consistent with the experimentally observed enantioselectivity (Table 7).

We observe that the selected docking poses exhibit a range of O–S distances between the substrate sulfur and the flavin (between 3.66 and 5.78 Å; see Table 7). We also note that the mutants corresponding to docking poses with distances greater than 5 Å (P440F, L443I, P440F/L443I, and I67Q/P440F/L443I) are those that are found experimentally to result in significant amounts of sulfone.

The single mutants P440F and L443I display higher conversion and enantioselectivity for (*S*)-**2b** than the WT enzyme. Both of these mutations result in a change in the shape of the active site pocket. The 443 residue lines the pocket, but while the 440 residue is on the same loop, it does not line the pocket. The L443I mutation hence changes the shape of the pocket directly, but the influence of the P440F mutation is exerted by reducing the backbone rigidity, enabling the movement of the loop containing L443 toward the pocket. The I67 side chain adopts a different conformation in these single mutants, compared to the WT enzyme, despite being on a different loop to the mutated residues. This may result in the change in shape of the active site. Because of the change in conformation of I67, both single mutants display a different binding pose of **1b** in the active site (Figure 9b and c), compared to the WT (Figure 9a), although in both cases these still favor formation of (*S*)-**2b**.

The double mutant P440F/L443I is also selective toward formation of (*S*)-**2b**; however, while the conversion is higher than in the case of the WT, the *ee* is smaller. The binding pose of **1b** in the double mutant (Figure 9d) is similar to that of the two single mutants (Figure 9b and c), and hence it is surprising that this double mutant shows a decrease in selectivity.

The triple mutant I67Q/P440F/L443I mutation is found experimentally to be selective toward formation of (*R*)-**2b**. In the binding pose shown in Figure 9e, the sulfur atom of **1b** is close to the Q67 NH_2 group, which may interact with the pro-(*S*) lone pair, thus leaving the pro-(*R*) lone pair available for reaction with the FAD moiety.

The quadruple mutant I67Q/P440F/A442N/L443I is the most (*R*)-selective mutant studied here. The additional A442N mutation results in a change in conformation about the –OOH moiety (Figure 9f). A hydrogen bond is formed between the Gln side chain carbonyl oxygen and the hydroperoxo hydrogen atom. This results in a different conformation of the R337 side chain, which forms a hydrogen bond to the same hydroperoxo group in the other mutants. This in turn allows **1b** to get closer to the hydroperoxo group in a position favoring oxidation of the (*R*)-lone pair and may explain the higher degree of (*R*)-enantioselectivity, compared to the triple mutant (I67Q/P440F/L443I).

It is clear from the experimental results that the P440F mutation is important for obtaining (*R*)-selectivity, as the triple mutant that does not contain this mutation (I67Q/A442N/L443I, Table 7) displays (*S*)-selectivity, although to a lesser extent than the WT. This is very interesting, considering that this mutation alone increases (*S*)-selectivity. The docking results described here support the importance of this mutation and also show the role of the additional mutations in achieving the high level of reversed (*R*)-selectivity.

Exploring Substrate Scope of the Evolved PAMO Mutants. The best (*R*)- and (*S*)-selective PAMO variants evolved for thioether **1b** were tested as catalysts in the asymmetric sulfoxidation of several other substrates **1a**, **4a–4c**, **7**, and **10** (Scheme 2), using purified enzymes. Since lysates and

dx.doi.org/10.1021/ja5098034 | J. Am. Chem. Soc. 2014, 136, 17262–17272

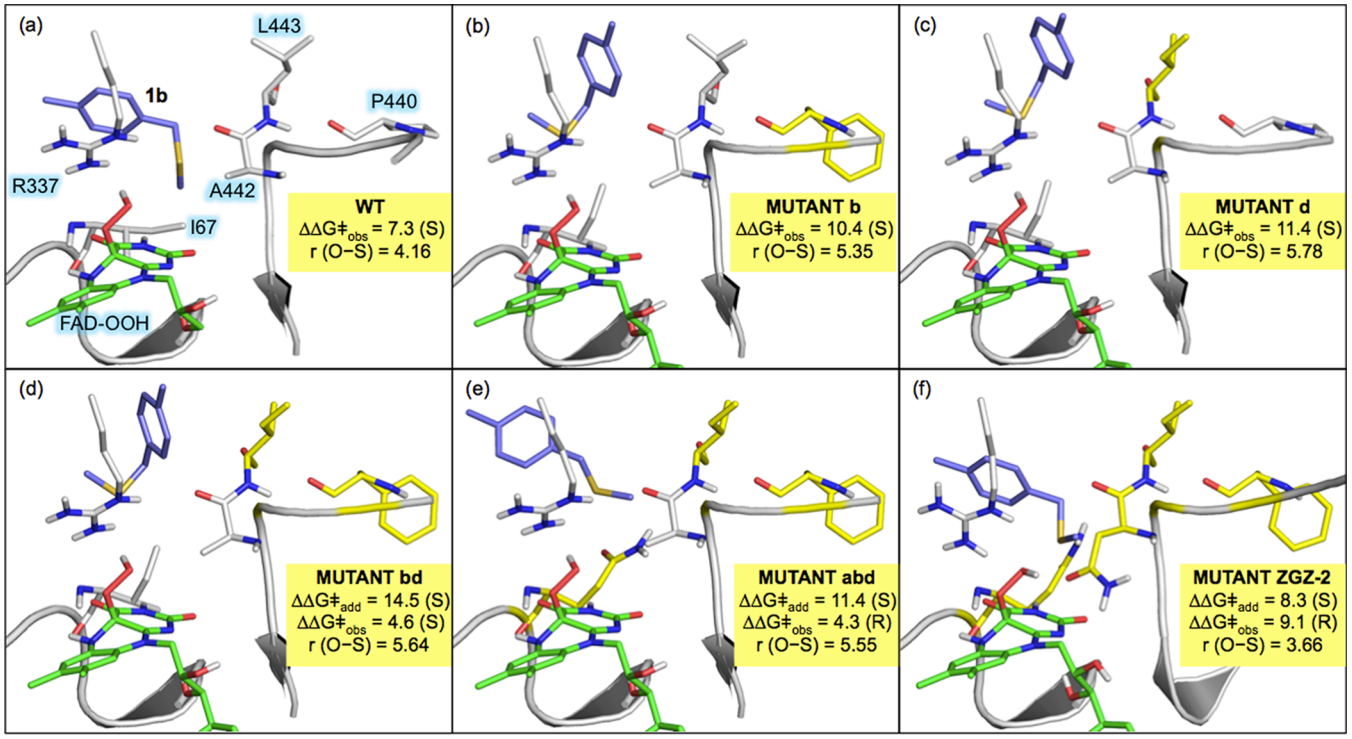

Figure 9. Induced fit docking results for substrate **1b** in (a) WT PAMO; (b) P440F; (c) L443I; (d) P440F/L443I; (e) I67Q/P440F/L443I; and (f) I67Q/P440F/A442N/L443I mutants. The mutated residues are displayed in yellow. Nonpolar hydrogen atoms are omitted for clarity. $-\Delta\Delta G^{\ddagger}$ values are given in kJ/mol, and r(O–S) in Å.

Scheme 2. Additional Substrates Used in PAMO-Catalyzed Asymmetric Sulfoxidation

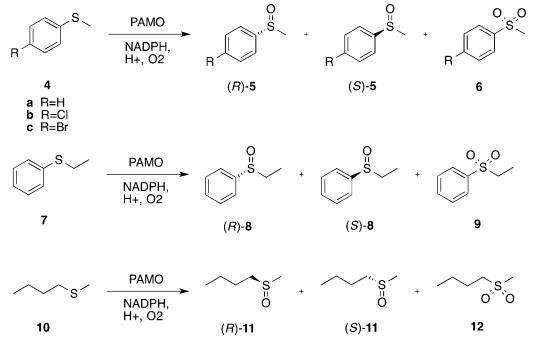

purified BVMO variants may lead to slightly different results in terms of *ee*-values and undesired overoxidation with formation of the respective sulfones, oxidation of the model thioether **1b** was included in this series of experiments. As already noted, when overoxidation occurs to a significant degree, kinetic resolution may influence the apparent *ee*-value of sulfoxidation. Fortunately, mutants having the highest stereoselectivity cause only small overoxidation. Highly (*R*)-selective variants for all of the thioethers were identified (>95% ee) except for **1a** (91% ee), while equally high (*S*)-selectivity proved to be possible only for substrates **1b**, **7**, and **10** (Table 8).

■ CONCLUSIONS AND PERSPECTIVES

In this study we have applied directed evolution to phenyl acetone monooxygenase (PAMO), a thermally robust Baeyer–Villiger monooxygenase, as a catalyst in the asymmetric sulfoxidation of prochiral thioethers. Since WT PAMO generally favors the formation of (*S*)-sulfoxides, emphasis was on the evolution of reversed enantioselectivity in favor of the (*R*)-products. This goal was reached (up to 95% *ee*) by knowledge-driven iterative saturation mutagenesis (ISM) with formation of high-quality mutant libraries requiring a minimum of screening (the bottleneck of directed evolution), with methyl-*p*-methylbenzyl thioether serving as the model substrate. WT PAMO shows 90% *ee* in favor of the (*S*)-sulfoxide, while the best (*R*)-selective mutant ZGZ-2, characterized by four point mutations I67Q/P440F/A442N/L443I, leads to 95% *ee*, which means a change in free energy of $\Delta\Delta G^{\ddagger}$ = 16.4 kJ/mol. This mutant also displays high enantioselectivity in the reaction of several other thioethers, and consequently constitutes an alternative to other catalysts in asymmetric sulfoxidation.[1−4] The four new point mutations do not impair the high thermostability of the enzyme, which is of practical importance. This also means that, if necessary, ZGZ-2 can be used as a template in future protein engineering studies.

An intriguing spinoff which emerged during our investigation concerns the question of additive versus nonadditive mutational effects.[12] Upon partial deconvolution of the most (*R*)-selective mutant I67Q/P440F/A442N/L443I (variant ZGZ-2) with generation of the four respective single mutants, it was discovered that all of them display the opposite sense of enantioselectivity in favor of the (*S*)-sulfoxide. This means that in concert four (*S*)-selective mutations lead to high (*R*)-selectivity. This prompted us to perform complete deconvolution by generating all combinatorial double and triple mutants. Here again strong cooperative nonadditive effects were observed. Using the experimental data, a designed fitness pathway landscape describing all 24 upward pathways leading from WT PAMO to the best mutant ZGZ-2 was constructed. Local minima were observed in 18 of the 24 trajectories, and in all of them pronounced cooperative nonadditive mutational

dx.doi.org/10.1021/ja5098034 | J. Am. Chem. Soc. 2014, 136, 17262−17272

Table 8. Performance of Selected Purified PAMO Mutants as Catalysts in Asymmetric Sulfoxidation Reactions

entry	substrate	variant	major product	% conversion	% ee	config.	% sulfone
1	**1a**	WT	**2a**	99	99	*S*	13
2	**1a**	ZGZ-1	**2a**	99	91	*R*	11
3	**1b**	Q152I	**2b**	81	97	*S*	4
4	**1b**	Q152V	**2b**	97	99	*S*	6
5	**1b**	Q152S	**2b**	66	96	*S*	6
6	**1b**	Q152M	**2b**	95	99	*S*	4
7	**1b**	Q152A	**2b**	78	97	*S*	5
8	**4a**	WT	**5a**	53	42	*R*	0
9	**4a**	P440L	**5a**	78	95	*R*	24
10	**4a**	I67A	**5a**	50	91	*S*	0
11	**4b**	WT	**5b**	83	9	*S*	4
12	**4b**	I67A	**5b**	93	94	*S*	15
13	**4b**	ZGZ-1	**5b**	99	99	*R*	9
14	**4b**	ZGZ-2	**5b**	99	94	*R*	8
15	**4b**	P440F/A442F/L443D	**5b**	99	95	*R*	20
16	**4b**	P440F/A442N/L443I	**5b**	99	90	*R*	11
17	**4c**	WT	**5c**	35	16	*S*	5
18	**4c**	I67A	**5c**	85	93	*S*	12
19	**4c**	ZGZ-1	**5c**	99	98	*R*	19
20	**4c**	ZGZ-2	**5c**	99	97	*R*	22
21	**4c**	P440F/A442F/L443D	**5c**	99	95	*R*	29
22	**4c**	P440F/A442N/L443I	**5c**	98	92	*R*	19
23	**7**	WT	**8**	63	12	*S*	7
24	**7**	P440L	**8**	42	97	*R*	0
25	**7**	ZGZ-1	**8**	98	93	*R*	18
26	**7**	A442D	**8**	88	96	*S*	10
27	**10**	WT	**11**	69	91	*S*	0
28	**10**	Q152S	**11**	81	94	*S*	0
29	**10**	Q152V	**11**	73	95	*S*	0
30	**10**	ZGZ-1	**11**	90	94	*R*	0
31	**10**	ZGZ-2	**11**	88	96	*R*	0

effects were found. The six energetically favored pathways that lack this feature likewise reveal synergistic mutational effects (nonadditivity).

In a previous study concerning the same type of analysis involving the epoxide hydrolase from *Aspergillus niger* as a catalyst in the hydrolytic kinetic resolution of a racemic epoxide, we constructed an analogous fitness landscape characterized by 5! = 120 pathways, with about half of them proving to be energetically favored due to the lack of local minima.[23] Thus, although ISM was applied in both cases in the evolution of the respective best mutant, the two landscapes differ somewhat in terms of the frequency of local minima. This result should be taken as yet another warning that experimental data derived from laboratory evolution should not be used to draw conclusions regarding the question of how many pathways in natural Darwinian evolution lead to fitter proteins.[12,23] To avoid confusion, it should be noted that fitness pathway landscapes obtained by deconvolution of a given evolved mutant as featured here and in a previous study[23] are fundamentally different from those that are constructed by studying experimentally and theoretically possible pathways in an ISM scheme.[14c]

The extreme synergistic mutational effects observed in the present study support once more the hypothesis that genetic changes in proteins are part of nonlinear systems.[12,23] Such effects are difficult to predict. Nevertheless, once observed, we were able to rationalize them by a theoretical analysis based on induced fit docking. Hopefully, insights of this type will someday lead to viable models with predictive power.

EXPERIMENTAL SECTION

Library Construction. Library A and B were created by the QuikChange method with the plasmid of the WT and corresponding mutants as a template. The primers used in the library creation process are listed in the Supporting Information (Table S3). The PCR reaction mixture contained the following: 10 × KOD Buffer (Novagen, 5 μL), Mg_2SO_4 (25 mM, 2 μL), dNTPs (2 mM each, 5 μL), template plasmid (20 ng/μL, 0.5 μL), KOD Polymerase (1 U). The PCR program contained an initial denaturation step at 95 °C for 3 min followed by 18 cycles of denaturation at 95 °C for 1 min, annealing at 72 °C for 1 min followed by elongation at 72 °C for 14 min. The final elongation at 72 °C for 35 min was then performed. The PCR product was digested by adding 5 units of DpnI at 37 °C for 4 h to remove the template plasmid. The treated PCR product was transformed into TOP 10 electrocompetent cells. The cells were spread on the LB-agar plates supplemented with 100 μg/mL carbenicilline for overnight incubation at 37 °C.

Library Screening. Individual colonies grown on the agar plates were placed into 96 deep-well plates containing 800 μL of LB media supplemented with 100 μg/mL carbenicilline. After overnight growth at 37 °C, with shaking at 800 rpm, 150 μL of LB culture were transferred into a 96-well plate containing 70 μL of 70% glycerol and mixed for preparation of glycerol stock plates. The glycerol stock plates were stored in a −80 °C freezer. 10 μL of each culture were used to inoculate a new plate containing 800 μL of TB media with 100 μg/mL of carbenicilline and 0.1% arabinose as an inducer for enzyme expression. The new inoculated plates were grown for an additional 20 h to express the PAMO enzyme at 30 °C, with shaking at 800 rpm.

dx.doi.org/10.1021/ja5098034 | J. Am. Chem. Soc. 2014, 136, 17262−17272

The cultures were centrifuged at 4000 rpm and at 4 °C for 15 min to collect cells. After discarding the supernatants, the cells in each well were suspended in 400 μL of 50 mM, pH 9.0 Tris-HCl buffer supplemented with 1 mg/mL lysozyme and 5 units of Dnase I. The plates were incubated at 37 °C with shaking at 800 rpm for 3 h and then centrifuged at 4 °C and 4000 rpm for 40 min.

100 μL of each supernatant were transferred into a new 96 deep-well plate to prepare the reaction mixture. In each well of the plate, 1 mL of reaction mixture was added, containing 5 mM Glucose-6-phosphate, 2 U glucose-6-phosphate dehydrogenase, 0.2 mM NADPH, and 2 mM substrate with 2% (v/v) acetonitrile. The reaction plates were incubated at 30 °C with shaking at 800 rpm for 6 h. After 600 μL of dichloromethane were added into each well, the reaction plates were centrifuged at 4 °C and 4000 rpm for 30 min. 300 μL of the organic layer in each well were transferred into 96 well plates and then filtered through 96 well filter plates with a 0.22 μL diameter (AcroPrep Advance 96 well Filter Plate). The organic layer was transferred into 96 well glass-made plates and was subjected to HPLC analysis. The mutants with improved selectivity were picked out, and the results were confirmed by repeating the reaction in Eppendorf tubes. The mutations in the gene of the mutants were confirmed by sequencing.

Enzyme Expression and Purification. The glycerol stocks of PAMO WT and mutants were inoculated into 4 mL of LB media supplemented with 100 μg/mL carbenicilline. After overnight growth at 37 °C, 2.5 mL of culture were transferred into 250 mL of TB media containing 100 μg/mL carbenicilline and 0.1 g/100 mL L-arabinose as an inducer at 30 °C with shaking at 200 rpm for 20 h for enzyme expression. Cell pellets were harvested by centrifugation and washed once with 50 mM, pH 9.0 Tris-HCl buffer. The pellets were suspended in 10 mL of 50 mM Tris-HCl buffer (pH 9.0) and were disrupted by sonication. The supernatant containing the crude enzyme was obtained by centrifugation at 4 °C and 12 000 rpm for 40 min. After going through the filter, the supernatant was subjected to affinity chromatography (GE Healthcare HisTrap FF Crude column) for purification. The impurity was removed by flushing the column with 25 mM imizadol, and the enzyme was eluted by 50 mM Tris-HCl buffer containing 200 mM imizadol and 0.5 M NaCl. The elution fractions were subjected to an Amicon Ultra-15 centrigugal filter for removal of salt and imizadol. The purified enzymes were dissolved in 50 mM, pH 9.0 Tris-HCl buffer and stored at −80 °C for use. The purity of the enzyme was confirmed by SDS-PAGE (Figure S1 in Supporting Information). The concentration of the purified enzyme was determined by a Bradford protein assay method, following the provided protocol.

Site-Directed Mutagenesis. The PAMO mutants were generated by using the QuikChange method,[20] following the protocol used in the library creation process. The only difference here is that primers with the targeted codon were used instead of degenerate primers. The primers used are summarized in the Supporting Information (Table S4). The targeted mutation in the gene of mutants was confirmed by sequencing.

General Procedure for the Biotransformation of Substrates. 2 mM of substrate were dissolved in 1 mL of 50 mM Tris-HCl buffer (pH 9.0), with 2% (v/v) acetonitrile as cosolvent. The reaction mixture contained 0.2 mM NADPH, 5 mM Glucose-6-phosphate, and 2 units of Glucose-6-phosphate dehydrogenase as the $NADP^+$ regeneration system. The reaction mixture was shaken at 1200 rpm and 30 °C for the times indicated. The reaction mixture was vigorously shaken after adding 300 μL of HPLC grade chloromethane to extract the product. After centrifugation at 4 °C for 30 min, the organic layer was extracted by syringe and filtered with a 0.22 μm filter (Whatman). The samples were analyzed by HPLC equipped with a Chiralcel OB-H column to determine the conversion of sulfides and the enantiomeric excesses of sulfoxides. The absolute configuration of the sulfoxide products was determined by comparison of their retention time with related literature or commercially available authentic compounds (Table S6 in Supporting Information).

Thermostability of PAMO Mutants. 40 μM of the purified mutant and WT enzyme were subjected to heating at 50, 52, 54, 56, 58, and 60 °C for 1 h. The samples were then put on ice for cooling for 10 min. The residual activities of the enzymes were determined at 30 °C, as above.

Kinetic Parameters. The purified enzymes were subjected to the determination of enzyme kinetic constants. The activity of the enzyme was measured by monitoring the consumption of NADPH at 25 °C and 340 nm (ε_{340} = 6.22 mM^{-1} cm^{-1}) during a fixed time. Each 1 mL reaction system consisted of 50 mM, Tris-HCl (pH 9.0), 100 μM NAPDH, 0.1−0.5 mM substrate, 2% (v/v) acetonitrile, and 0.05−0.5 μM purified enzyme. The measurements were performed by using the Molecular Devices Spectramax. The data from the spectrophotometric assay were used to calculate the kinetic constants of enzymes using the Michaelis−Menten equation.

Molecular Docking Calculations. Docking was performed using the Induced Fit Docking procedure developed by Schrödinger.[25] The crystal structure of PAMO containing FAD and NADP was used (PDB entry 2YLR).[15] The receptor model was built using the Protein Preparation Wizard.[26] Protonation states were determined using PROPKA.[27] Prior to docking, each protein structure was energy minimized using the OPLS2005 force field,[28] with all heavy atoms restrained to an RMSD of 0.3 Å.

■ ASSOCIATED CONTENT

Ⓢ Supporting Information

Reaction data from additional PAMO mutants, primers used for library creation and site-directed mutagenesis, chiral HPLC separation conditions, thermodynamic analysis for deconvolution of mutants, and detailed results from Induced Fit Docking calculations. This material is available free of charge via the Internet at http://pubs.acs.org.

■ AUTHOR INFORMATION

Corresponding Author

reetz@mpi-muelheim.mpg.de

Notes

The authors declare no competing financial interest.

■ ACKNOWLEDGMENTS

Financial support by the Max-Planck-Society and the Arthur C. Cope Foundation is gratefully acknowledged.

■ REFERENCES

(1) Recent key reviews and studies of transition metal catalyzed asymmetric sulfoxidation: (a) Kagan, H. B. In *Organosulfur Chemistry in Asymmetric Synthesis*; Toru, T., Bolm, C., Eds.; Wiley-VCH: Weinheim, 2009; pp 1−29. (b) Pelllissier, H. *Tetrahedron* **2006**, *62*, 5559−5601. (c) Kaczorowska, K. B.; Kolarska, Z.; Mitka, M.; Kowalski, P. *Tetrahedron* **2005**, *61*, 8315−8327. (d) Liao, S.; List, B. *Adv. Synth Catal.* **2012**, *354*, 2363−2367. (e) Legros, J.; Bolm, C. *Angew. Chem., Int. Ed.* **2004**, *43*, 4225−4228. (f) Legros, J.; Bolm, C. *Chem.—Eur. J.* **2005**, *11*, 1086−1092. (g) Fukisaki, J.; Matsumoto, K.; Matsumoto, K.; Katsuki, T. *J. Am. Chem. Soc.* **2011**, *133*, 56−61. (h) Capozzi, M. A.; Capitelli, F.; Bottoni, A.; Calvaresi, M.; Cardellicchio, C. *ChemCatChem* **2013**, *5*, 210−219. (i) O'Mahoney, G. E.; Ford, A.; Maguire, A. R. *J. Org. Chem.* **2012**, *77*, 3288−3296. (j) Newhouse, T. R.; Li, X.; Blewett, M. M.; Whitehead, C.; Clare, M. C.; Corey, E. J. *J. Am. Chem. Soc.* **2012**, *134*, 17354−17357.

(2) Recent key reviews and studies of organocatalytic asymmetric sulfoxidation: (a) Jurok, R.; Hodačová, J.; Eigner, V.; Dvořáková, H.; Setnička, V.; Cibulka, R. *Eur. J. Org. Chem.* **2013**, 7724−7738. (b) Russo, A.; De Fusco, C.; Lattanzi, A. *ChemCatChem* **2012**, *4*, 901−916. (c) Stingl, K. A.; Tsogoeva, S. B. *Tetrahedron: Asymmetry* **2010**, *21*, 1055−1074. (c) Bäckvall, J.-E. In *Modern Oxidation Methods*; Bäckvall, J.-E., Eds.; Wiley-VCH: Weinheim, 2010; pp 277−313. (d) Armstrong, A. In *Enantioselective Organocatalysis*; Dalko, P. I., Eds.; Wiley-VCH: Weinheim, 2007; pp 403−424. (e) Imada, Y.; Kitagawa, T.; Wang, H.-K.; Komiya, N.; Naota, T. *Tetrahedron Lett.* **2013**, *54*,

621−624. (f) Ménová, P.; Cibulka, R. *J. Mol. Catal. A* **2012**, *363*−*364*, 362−370. (g) Lindén, A. A.; Hermanns, N.; Ott, S.; Krüger, L.; Bäckvall, J.-E. *Chem.—Eur. J.* **2005**, *11*, 112−119. (h) Imada, Y.; Iida, H.; Murahashi, S.-I. *Angew. Chem., Int. Ed.* **2005**, *44*, 1704−1706. (i) Liao, S.; Coric, I.; Wang, Q.; List, B. *J. Am. Chem. Soc.* **2012**, *134*, 10765−10768.

(3) Reviews of structure, mechanism, protein engineering and applications of BVMOs: (a) Walsh, C. T.; Chen, Y.-C. J. *Angew. Chem.* **1988**, *100*, 342−352. (b) Orru, R.; Dudek, H. M.; Martinoli, C.; Torres Pazmiño, D. E.; Royant, A.; Weik, M.; Fraaije, M. W. *J. Biol. Chem.* **2011**, *286*, 29284−29291. (c) Kayser, M. M. *Tetrahedron* **2009**, *65*, 947−974. (d) Mihovilovic, M. D.; Drauz, K.; Gröger, H.; May, O. *Enzyme Catalysis in Organic Synthesis*, Vols. *I*−*III*, 3rd ed.; Wiley-VCH: Weinheim, 2012; pp 1439−1485. (e) Mihovilovic, M. D. *Curr. Org. Chem.* **2006**, *10*, 1265−1287. (f) Wohlgemuth, R. *Eng. Life Sci.* **2006**, *6*, 577−583. (g) Leisch, H.; Morley, K.; Lau, P. *Chem. Rev.* **2011**, *111*, 4165−4222. (h) Hollmann, F.; Arends, I. W. C. E.; Buehler, K.; Schallmey, A.; Bühler, B. *Green Chem.* **2011**, *13*, 226−265. (i) Balke, K.; Kadow, M.; Mallin, H.; Saß, S.; Bornscheuer, U. T. *Org. Biomol. Chem.* **2012**, *10*, 6249−6265. (j) Zambianchi, F.; Pasta, P.; Colonna, S.; Gaggero, N.; Woodley, J. M. *Biotechnol. Bioeng.* **2002**, *78*, 489−496.

(4) Reviews and key papers of BVMO-catalyzed asymmetric sulfoxidation: (a) Matsui, T.; Dekishima, Y.; Ueda, M. *Appl. Microb. Biotechnol.* **2014**, *98*, 7699−7706. (b) Riebel, A.; de Gonzalo, G.; Fraaije, M. W. *J. Mol. Catal. B* **2013**, *88*, 20−25. (c) Bisagni, S.; Summers, B.; Kara, S.; Hatti-Kaul, R.; Grogan, G.; Mamo, G.; Hollmann, F. *Top. Catal.* **2014**, *57*, 366−375.

(5) Polyak, I.; Reetz, M. T.; Thiel, W. *J. Am. Chem. Soc.* **2012**, *134*, 2732−2741.

(6) Reetz, M. T.; Daligault, F.; Brunner, B.; Hinrichs, H.; Deege, A. *Angew. Chem., Int. Ed.* **2004**, *43*, 4078−4081.

(7) (a) Fraaije, M. W.; Wu, J.; Heuts, D. P. H. M.; van Hellemond, E. W.; Spelberg, J. H. L.; Janssen, D. B. *Appl. Microbiol. Biotechnol.* **2005**, *66*, 393−400. (b) Zambianchi, F.; Fraaije, M. W.; Carrea, G.; de Gonzalo, G.; Rodriguez, C.; Gotor, V.; Ottolina, G. *Adv. Synth. Catal.* **2007**, *349*, 1327−1331. (c) Rodriguez, C.; de Gonzalo, G.; Torres Pazmiño, D. E.; Fraaije, M. W.; Gotor, V. *Tetrahedron: Asymmetry* **2008**, *19*, 197−203. (d) Zhang, Z.-G.; Parra, L. P.; Reetz, M. T. *Chem.—Eur. J.* **2012**, *18*, 10160−10172.

(8) WT PAMO as a sulfoxidation catalyst: de Gonzalo, G.; Torres Pazmiño, D. E.; Ottolina, G.; Fraaije, M. W. *Tetrahedron: Asymmetry* **2005**, *16*, 3077−3083.

(9) Malito, E.; Alfieri, A.; Fraaije, M. W.; Mattevi, A. *Proc. Natl. Acad. Sci. U.S.A.* **2004**, *101*, 13157−13162.

(10) Torres Pazmiño, D. E.; Snajdrova, R.; Rial, D. V.; Mihovilovic, M. D.; Fraaije, M. W. *Adv. Synth. Catal.* **2007**, *349*, 1361−1368.

(11) Reviews of directed evolution: (a) *Directed Evolution Library Creation*, 2nd ed.; Gillam, E. M. J., Copp, J. N., Ackerley, D. F., Eds.; Methods in Molecular Biology; Humana Press: Totowa, 2014. (b) Widersten, M. *Curr. Opin. Chem. Biol.* **2014**, *21*, 42−47. (c) Siloto, R. M. P.; Weselake, R. J. *Biocatal. Agric. Biotechnol.* **2012**, *1*, 181−189. (d) Goldsmith, M.; Tawfik, D. S. *Curr. Opin. Struct. Biol.* **2012**, *22*, 406−412. (e) Cobb, R. E.; Chao, R.; Zhao, H. *AIChE J.* **2013**, *59*, 1432−1440. (f) Reetz, M. T. Directed evolution of enzymes. In *Enzyme Catalysis in Organic Synthesis*; Drauz, K., Dröge, H., May, O., Eds.; Wiley-VCH: Weinheim, 2012; Vol. *1*, pp 119−190. (g) Bommarius, A. S.; Blum, J. K.; Abrahamson, M. J. *Curr. Opin. Chem. Biol.* **2011**, *15*, 194−200. (h) Quin, M. B.; Schmidt-Dannert, C. *ACS Catal.* **2011**, *1*, 1017−1021. (i) Brustad, E. M.; Arnold, F. H. *Curr. Opin. Chem. Biol.* **2011**, *15*, 201−210. (j) Jäckel, C.; Hilvert, D. *Curr. Opin. Biotechnol.* **2010**, *21*, 753−759. (k) Turner, N. J. *Nat. Chem. Biol.* **2009**, *5*, 567−573. (l) Lutz, S.; Bornscheuer, U. T. *Protein Engineering Handbook*; Wiley-VCH: Weinheim, 2009; Vols. *1*−*2*.

(12) Reetz, M. T. *Angew. Chem., Int. Ed.* **2013**, *52*, 2658−2666.

(13) Directed evolution studies of PAMO as the catalyst in asymmetric Baeyer−Villiger reactions: (a) Parra, L. P.; Agudo, R.; Reetz, M. T. *ChemBioChem* **2013**, *14*, 2301−2309. (b) Zhang, Z.-G.; Roiban, G.-D.; Acevedo, J. P.; Polyak, I.; Reetz, M. T. *Adv. Synth. Catal.* **2013**, *355*, 99−106. (c) Wu, S.; Acevedo, J. P.; Reetz, M. T. *Proc. Natl. Acad. Sci. U.S.A.* **2010**, *107*, 2775−2780. (d) Reetz, M. T.; Wu, S. *Chem. Commun.* **2008**, 5499−5501.

(14) (a) Reetz, M. T. *Angew. Chem., Int. Ed.* **2011**, *50*, 138−174. (b) Acevedo-Rocha, C. G.; Kille, S.; Reetz, M. T. In *Directed Evolution Library Creation: Methods and Protocols*, 2nd ed.; Ackerley, D., Copp, J., Gillam, E., Eds.; Methods in Molecular Biology; Humana Press: Totowa, 2014. (c) Gumulya, Y.; Sanchis, J.; Reetz, M. T. *ChemBioChem* **2012**, *13*, 1060−1066.

(15) Orru, R.; Dudek, H. M.; Martinoli, C.; Torres Pazmino, D. E.; Royant, A.; Weik, M.; Fraaije, M. W.; Mattevi, A. *J. Biol. Chem.* **2011**, *286*, 29284−29291.

(16) (a) Tang, L.; Gao, H.; Zhu, X.; Wang, X.; Zhou, M.; Jiang, R. *BioTechniques* **2012**, *52*, 149−158. (b) Kille, S.; Acevedo-Rocha, C. G.; Parra, L. P.; Zhang, Z.-G.; Opperman, J. J.; Reetz, M. T.; Acevedo, J. P. *ACS Synth. Biol.* **2013**, *2*, 83−92.

(17) Patrick, W. M.; Firth, A. E. *Biomol. Eng.* **2005**, *22*, 105−112.

(18) (a) Carter, D. C.; Winter, G.; Wilkinson, A. J.; Fersht, A. R. *Cell* **1984**, *38*, 835−840. (b) Wells, J. A. *Biochemistry* **1990**, *29*, 8509−8517. (c) See also: Mildvan, A. S.; Weber, D. J.; Kuliopulos, A. *Arch. Biochem. Biophys.* **1992**, *294*, 327−340.

(19) Early examples of nonadditive mutational effects: (a) Serrano, L.; Horovitz, A.; Avron, B.; Bycroft, M.; Fersht, A. R. *Biochemistry* **1990**, *29*, 9343−9352. (b) Huang, Z.; Wagner, C. R.; Benkovic, S. J. *Biochemistry* **1994**, *33*, 11576−11585. (c) Wagner, C. R.; Huang, Z.; Singleton, S. F.; Benkovic, S. J. *Biochemistry* **1995**, *34*, 15671−15680.

(20) Recent examples of nonadditive mutational effects: (a) Reetz, M. T.; Prasad, S.; Carballeira, J. D.; Gumulya, Y.; Bocola, M. *J. Am. Chem. Soc.* **2010**, *132*, 9144−9152. (b) Zheng, H.; Reetz, M. T. *J. Am. Chem. Soc.* **2010**, *132*, 15744−15751. (c) Sandström, A. G.; Wikmark, Y.; Engström, K.; Nyhlén, J.; Bäckvall, J.-E. *Proc. Natl. Acad. Sci. U.S.A.* **2012**, *109*, 78−83. (d) Bartsch, S.; Kourist, R.; Bornscheuer, U. T. *Angew. Chem.* **2008**, *120*, 1531−1534. (e) Istomin, A. Y.; Gromiha, M. M.; Vorov, O. K.; Jacobs, D. J.; Livesay, D. R. *Proteins: Struct., Funct., Bioinf.* **2007**, *70*, 915−924.

(21) Hogrefe, H. H.; Cline, J.; Youngblood, G. L.; Allen, R. M. *BioTechniques* **2002**, *33*, 1158−1165.

(22) Reetz, M. T.; Carballeira, J. D.; Peyralans, J.; Höbenreich, H.; Maichele, A.; Vogel, A. *Chem.—Eur. J.* **2006**, *12*, 6031−6038.

(23) Reetz, M. T.; Sanchis, J. *ChemBioChem* **2008**, *9*, 2260−2267.

(24) Polyak, I.; Reetz, M. T.; Thiel, W. *J. Phys. Chem. B* **2013**, *117*, 4993−5001.

(25) (a) Schrödinger Suite 2014−2 Induced Fit Docking protocol; Glide version 6.3, Schrödinger, LLC, New York, NY, 2013; Prime version 3.6, Schrödinger, LLC: New York, NY, 2014. (b) Farid, R.; Day, T.; Friesner, R. A.; Pearlstein, R. A. *Bioorg. Med. Chem.* **2006**, *14*, 3160−3173. (c) Sherman, W.; Day, T.; Jacobson, M. P.; Friesner, R. A.; Farid, R. *J. Med. Chem.* **2006**, *49*, 534−553. (d) Sherman, W.; Beard, H. S.; Farid, R. *Chem. Biol. Drug Des.* **2006**, *67*, 83−84.

(26) (a) Schrödinger Suite 2014−2 Protein Preparation Wizard; Epik version 2.8; Schrödinger, LLC: New York, NY, 2014; Impact version 6.3; Schrödinger, LLC: New York, NY, 2014; Prime version 3.5; Schrödinger, LLC: New York, NY, 2014. (b) Sastry, G. M.; Adzhigirey, M.; Day, T.; Annabhimoju, R.; Sherman, W. *J. Comput. Aid. Mol. Des.* **2013**, *27* (3), 221−234.

(27) (a) Li, H.; Robertson, A. D.; Jensen, J. H. *Proteins* **2005**, *61*, 704−721. (b) Bas, D. C.; Rogers, D. M.; Jensen, J. H. *Proteins* **2008**, *73*, 765−783. (c) Olsson, M. H. M.; Søndergard, C. R.; Rostkowski, M.; Jensen, J. H. *J. Chem. Theory Comput.* **2011**, *7*, 525−537. (d) Søndergaard, C. R.; Olsson, M. H. M.; Rostkowski, M.; Jensen, J. H. *J. Chem. Theory Comput.* **2011**, *7*, 2284−2295.

(28) Banks, J. L.; Beard, H. S.; Cao, Y.; Cho, A. E.; Damm, W.; Farid, R.; Felts, A. K.; Halgren, T. A.; Mainz, D. T.; Maple, J. R.; Murphy, R.; Philipp, D. M.; Repasky, M. P.; Zhang, L. Y.; Berne, B. J.; Friesner, R. A.; Gallicchio, E.; Levy, R. M. *J. Comput. Chem.* **2005**, *26*, 1752−1780.